Influence of Photochemical Loss of VOCs on Understanding Ozone Formation Mechanism

Wei Ma[1], Zemin Feng[1], Junlei Zhan[1], Yongchun Liu[1*], Pengfei Liu[2,4,5], Chengtang Liu[2,4,5], Qingxin Ma[2,4,5],

Kang Yang[3], Yafei Wang[3], Hong He[2,4,5], Markku Kulmala[1,6], Yujing Mu[2,4,5], Junfeng Liu[2,4,5*]

1. Aerosol and Haze Laboratory, Advanced Innovation Center for Soft Matter Science and Engineering,

Beijing University of Chemical Technology, Beijing, 100029, China

2. Research Center for Eco-Environmental Sciences, Chinese Academy of Sciences, Beijing, 100085, China

3. Beijing Institute of Petrochemical Technology, Beijing 102617, China

4. Center for Excellence in Regional Atmospheric Environment, Institute of Urban Environment, Chinese

Academy of Sciences, Xiamen 361021, China

5. University of Chinese Academy of Sciences, Beijing 100049, China

6. Institute for Atmospheric and Earth System Research, Faculty of Science, University of Helsinki, Helsinki,

00014, Finland

*Corresponding to: Yongchun Liu (liuyc@buct.edu.cn) and Junfeng Liu (junfengliu@rcees.ac.cn)

Abstract

Volatile organic compounds (VOCs) tend to be consumed by atmospheric oxidants, resulting in substantial photochemical loss during transport. An observation-based model was used to evaluate the influence of photochemical loss of VOCs on the sensitivity regime and mechanisms of ozone formation. Our results showed that a VOC-limited regime based on observed VOC concentrations shifted to a transition regime with a photochemical initial concentration of VOCs (PIC-VOCs) in the morning. The net ozone formation rate was underestimated by 3 ppb h^{-1} (~36 ppb day^{-1}) based on the PIC-VOCs. The relative contribution of the RO_2 path to ozone production based on the PIC-VOCs accordingly increased by 13.4%; in particular, the contribution of alkene-derived RO_2 increased by approximately 10.2%. In addition, the OH-HO_2 radical cycle was obviously accelerated by highly reactive alkenes after accounting for photochemical loss of VOCs. The contribution of local photochemistry might be underestimated for both local and regional ozone pollution if consumed VOCs are not accounted for, and policymaking on ozone pollution prevention should focus on VOCs with a high reactivity.

1. Introduction

Ground surface ozone (O_3) is an important atmospheric pollutant that is harmful to human health and is connected with respiratory, cardiovascular diseases, and premature mortality (Cohen et al., 2017). It is also harmful to vegetation growth. For example, it led to annual reductions in the yields of rice and wheat by 8% and 6%, respectively, and reduced forest biomass growth by 11-13% in China (Feng et al., 2019). Surface O_3 concentrations have increased by 11.9% over eastern China despite the air pollution control measures implemented in China from 2012 to 2017 (Dang and Liao, 2019). An economic loss of 0.09% of the Chinese gross domestic product (78 billion CNY) is predicted for 2030 if policies against O_3 pollution are not properly implemented (Xie et al., 2019). Therefore, urgent action to minimize O_3 pollution in China is needed.

Tropospheric O_3 is mainly produced from photochemical reactions between volatile organic compounds (VOCs) and nitrogen oxides (NO_x: $NO+NO_2$) (Seinfeld and Pandis, 2006; Liu et al., 2021). O_3 is generated from a collision of O_2 and $O(3P)$ that is produced from photolysis of NO_2 in the atmosphere. Peroxyl radicals (HO_2 and RO_2), which are produced from the oxidation of VOCs by OH radical, can efficiently convert NO (from the photolysis of NO_2) to NO_2, leading to a net O_3 production by compensating for the titration of O_3 by NO (Monks, 2005; Zhang et al., 2021a). Over the past two decades, a number of field observations focused on O_3 pollution levels and its precursors have been carried out in the Beijing-Tianjin-Hebei (BTH), Yangtze River Delta (YRD), and Pearl River Delta (PRD) regions (Wang et al., 2017; Li et al., 2019; Xue et al., 2014; Zhang et al., 2019). Due to the nonlinear relationship

53   between O_3 and its precursors and the variations in meteorological conditions, numerous

54   studies have been performed to understand the sensitivity regime of O_3 formation (Ling and

55   Guo, 2014; Zhang et al., 2020), the photochemical process of O_3 formation based on box

56   models or observation-based models (OBM) (He et al., 2019; Tan et al., 2019), and the sources

57   of O_3 using regional chemical transport models (Li et al., 2016b; Li et al., 2016c). Recently,

58   the instantaneous production rate of the O_3 formation process has attracted more attention; for

59   example, studies examining radical recycling ($OH\text{-}RO_2\text{-}RO\text{-}HO_2\text{-}OH$) related to the production

60   of O_3 have been performed (Lu et al., 2017; Tan et al., 2017; Whalley et al., 2018). HCHO

61   photolysis and alkene ozonolysis contributed approximately 85% to the primary production of

62   HO_2 and HO radicals in Beijing, Shanghai and Guangzhou (Tan et al., 2019; Yang et al., 2017).

63   The importance of HONO and HCHO photolysis for primary radical production has also been

64   proposed in suburban and rural areas (Tan et al., 2017; Lu et al., 2012; Lu et al., 2013).

65   All of the OBM studies investigating the relationship between O_3 and VOCs were based

66   on measured datasets. However, VOCs are highly reactive to atmospheric oxidants, such as

67   OH, NO_3, and O_3, among which OH is dominant. The lifetimes of some highly reactive VOCs,

68   such as isoprene, are as short as only a few tens of minutes under typical daytime atmospheric

69   conditions. The mixing ratios of VOCs observed at a sampling site are actually the residues of

70   VOCs from emissions due to the photochemical loss during transport from the source site to

71   the receptor site. If photochemically consumed VOCs are not considered, the O_3 formation

72   sensitivity and net O_3 production may be misunderstood, and subsequent policymaking on O_3

73   pollution prevention at regional or urban scales may be misguided. Thus, the photochemical

74   age-based approach has been applied to evaluate the effect of photochemical processes on VOC

75   measurements (Shao et al., 2011). This method was used to qualitatively or semi-quantitatively

76   estimate the O_3 formation process of the source-receptor (Gao et al., 2018) by calculating the

77   O_3 formation potential (OFP) (Han et al., 2017), identifying the critical species for O_3 formation

78   (Gao et al., 2021), or evaluating the VOC emissions ratio (Yuan et al., 2013). In evaluating the

79   importance of initial VOCs to ozone production, Xie et al. (2008) found that the OFP at a

80   Peking University site increased by 70% after accounting for the photochemical loss of VOCs.

81   Li et al. (2015) also showed that the OFPs of total NMHCs (excluding isoprene) increased by

82   16.1% (from 59.6 to 69.2 ppb O_3), 12.1% (from 33.5 to 37.5 ppb O_3), and 3.4% (from 68.9 to

83   71.2 ppb O_3) after correcting for photochemical loss in Gucheng, Quzhou, and Beijing,

84   respectively. Gao et al. (2018) reported that the OFP could be underestimated by 23.4% (62.4

85   ppb O_3) in Beijing if the photochemical loss of VOCs is not considered. Zhan et al. (2021)

86   found that based on measured VOCs, the OFP increased from 57.8 ppb to 103.9 ppb using the

87   initial VOCs. All the previous work was based on the maximum incremental reactivities (MIR)

88   method. However, the application of such calculations using the MIR method is restricted to

89   areas or episodes in which O_3 formation is VOC-sensitive (Carter, 1994). In the troposphere,

90   the sensitivity of ozone formation to NOx and VOCs varies greatly, as evidenced by the wide

91   range of OFP underestimations from ~3% to 70% in previous work. Thus, the nonlinear

92   relationship between ozone and VOCs/NOx cannot be well described using the MIR method,

93   and a quantitative analysis is necessary to explicitly understand the ozone formation process

94   and its mechanisms in the atmosphere.

95   In this study, an OBM was used to evaluate the local O_3 formation process in summer in

96   Beijing based on concentrations of observed and photochemical initial concentrations of VOCs

97   (PIC-VOCs). The O_3-NO_x-VOC sensitivity, instantaneous O_3 formation rate and in situ O_3

98   formation process were discussed. The aim of this study was to understand the possible

99   influence of photochemical loss of VOCs on the formation sensitivity regime of O_3 and how

100   the photochemical loss of VOCs affects O_3 formation. This study can provide new insight for

101   better understanding atmospheric O_3 pollution.

102 2. Methodology

103 2.1 Experimental section

104   Field observations were carried out on the Qingyuan campus of the Beijing Institute of

105   Petrochemical Technology (BIPT, 39.73°N and 116.33°E) (Figure S1). Details on the

106   observation site have been described in our previous work (Zhan et al., 2021). In short, the site

107   is a typical suburban site in the Daxing District between 5th Ring Road and 6th Ring Road. The

108   field campaign was carried out during August 1-28, 2019, when photochemistry was the most

109   active and rainfall was rare in Beijing.

110   The concentrations of nonmethane hydrocarbons (NMHCs) were detected by both a gas

111   chromatography-flame ionization detector (GC/FID) and a single photon ionization (SPI) TOF-

112   MS (SPI-MS 3000, Guangzhou Hexin Instrument Co., Ltd., China). A detailed description of

113   the instrumentation can be found in previous publications (Zhan et al., 2021; Chen et al., 2020).

114   The SPI-MS was also used to detect halohydrocarbons. More details on this instrument and its

115   parameter settings have been described in previous studies (Zhang et al., 2019; Liu et al.,

116   2020a). In short, a 0.002 int thick polydimethylsiloxane (PDMS) membrane (Technical

117   Products Inc., USA) was used to collect VOCs and diffuse them from the sample site to the

118   detector under high vacuum conditions. Vacuum ultraviolet (VUV) light generated by a

119   commercial D2 lamp (Hamamatsu, Japan) was utilized for ionization at 10.8 eV. For ion

120   detection, two microchannel plates (MCPs, Hamamatsu, Japan) assembled with a chevron-type

121   configuration were employed. This TOF-MS has an LOD varying from 50 ppt to 1 ppb with a

122   1-minute time resolution for most trace gases without any preconcentration procedure. To

123   verify the data compatibility of the SPIMS and GC/FID, we compared the concentrations of

124   toluene measured using these two different instruments (Figure S2). The correlation coefficient

125   was 0.9 (with a slope of 0.7), indicating that the concentrations of NMHCs were comparable

126   using these two measurement techniques.

127   Oxygenated VOCs (OVOCs) were collected using 2,4-dinitrophenylhydrazine (DNPH)-

128   coated silica gel cartridges (Sep-Pak, Waters) by an automatic sampling device with a sampling

129   flow rate of 1.2 L min^{-1} and a duration of 2 h for each sample. Then, the OVOCs were analysed

130   using high-performance liquid chromatography (HPLC, Inertsil ODS-P 5 μm 4.6 × 250 mm

131   column, GL Sciences) with an acetonitrile-water binary mobile phase (Ma et al., 2019). To

132   avoid possible contamination or desorption after sampling, cartridges were capped, placed into

133   tightly closed plastic bags and kept in a refrigerator before analysis. The sampled cartridges

134   were eluted with 5 mL acetonitrile and analysed by HPLC as soon as possible after they were

135   shipped back to the laboratory. This system was calibrated with 8-gradient standard solutions

136   (TO11/IP-6A Aldehyde/Ketone-DNPH Mix, SUPELCO). The correlation coefficients were all

137 greater than 0.999. The LOD for most OVOCs was approximately 10 ppt.

138   Trace gases, including NOx, SO$_2$, CO, and O$_3$, were measured using corresponding

139 analysers (Thermo Scientific, 42i, 43i, 48i, and 49i, respectively). The HONO concentration

140 was measured using a homemade long path absorption photometer (LOPAP) (Liu et al., 2020c).

141 The meteorological parameters, including temperature (T), pressure (P), relative humidity

142 (RH), wind speed, and wind direction, were measured by a weather station (AWS310, Vaisala).

143 The photolysis rate (J_{NO2}) was measured via continuous measurement of the actinic flux in the

144 wavelength range of 285-375 nm using a J_{NO2} filter radiometer (J_{NO2} radiometer, Metcon).

145 **2.2 Calculation of photochemical loss of VOCs**

146   The photochemical loss of VOCs was calculated using the ratio method (Wiedinmyer et

147 al., 2001; Yuan et al., 2013). The initial mixing ratio of a specific VOC was calculated using

148 the following equations (Mckeen et al., 1996):

149
$$[VOC_i]_t = [VOC_i]_{t0} \times \exp(-k_i \times [OH] \times \Delta t) \quad (1)$$

150
$$\Delta t = \frac{1}{[OH] \times (k_X - k_E)} \times \left\{ ln\left(\frac{X_0}{E_0}\right) - ln\left(\frac{X_t}{E_t}\right) \right\} \quad (2)$$

151 where $[VOC_i]_t$ and $[VOC_i]_{t0}$ are the observed and initial concentrations of VOC_i, respectively;

152 k_i is the second-order reaction rate between compound i and OH radical; and $[OH]$ and Δt are

153 the concentration of OH radical and the photochemical ageing time, respectively. k_X and k_E are

154 rate constants for the reaction between OH radicals and xylene (7.00×10^{-12} cm^3 molecule^{-1} s^{-1})

155 and ethylbenzene (1.87×10^{-11} cm^3 molecule^{-1} s^{-1}) (Atkinson and Arey, 2003), respectively.

156 (X_0/E_0) is the initial mixing ratio between xylene and ethylbenzene, and (X_t/E_t) is the mixing

157 ratio between xylene and ethylbenzene at the observation time. In this study, we chose the mean

158   concentrations of xylene and ethylbenzene at 05:00-06:00 as their initial concentrations before

159   sunrise according to the ambient J_{NO2} (Figure S3) to calculate the photochemical loss of OH

160   exposure. In previous work (Shao et al., 2011; Zhan et al., 2021), the selection of ethylbenzene

161   and xylene as tracers was justified for calculating ambient OH exposure under the following

162   conditions: 1) the concentrations of xylene and ethylbenzene were well correlated (Figure S4),

163   which indicated that they were simultaneously emitted; 2) they had different degradation rates

164   in the atmosphere; and 3) the calculated PICs were in good agreement with those calculated

165   using other tracers, such as i-butene/propene (Zhan et al., 2021). To test the relative constant

166   emission ratio from different sources, we chose benzene vs. acetylene and n-hexane vs. toluene

167   as references, and the result is shown in Figure S5. These ambient ratios could directly reflect

168   their relative emission rates from sources (Goldan et al., 2000; Jobson et al., 2004). The linear

169   correlation coefficients (R^2) were generally higher than 0.7, which were equal to that reported

170   by Shao et al. (2011). To further test the assumption that the emissions of xylene and

171   ethylbenzene were constant throughout the day, their potential sources were calculated using a

172   source-receptor model (the potential source contribution function, PSCF). As shown in Figure

173   S6, xylene and ethylbenzene showed similar distributions. In addition, the ratio of

174   ethylbenzene/xylene at 5:00 and 6:00 was similar to that during the daytime. These results

175   indicated that the emissions of xylene and ethylbenzene were constant throughout the day. The

176   ratio of xylene to ethylbenzene and the OH exposure concentration are shown in Figure S7.

177   The results showed that the ratio of xylene to ethylbenzene increased gradually (07:00~12:00),

178   which is consistent with the trend of xylene and ethylbenzene. The OH exposure was from 0.82

179   to 8.1×10^6 molecule cm^{-3} h, with a mean daytime value of $4.3\pm1.9\times10^6$ molecules cm^{-3} h.

180   Accordingly, the mean photochemical ages were 1.7 ± 0.9 h using the mean daytime (8:00-17:00

181   LT) OH concentrations ($4.3\pm3.1\times10^6$ molecules cm^{-3}) calculated based on JO1D using the

182   method reported in our previous work (Liu et al., 2020b; Liu et al., 2020c). This meant that

183   VOCs would undergo obvious degradation even during a short range of transport in the

184   atmosphere.

185   It should be noted that the k_{OH} of isoprene is 9.98×10^{-11} cm^3 molecule^{-1} s^{-1} at 298.15 K

186   (Atkinson and Arey, 2003), almost two orders of magnitude greater than other VOCs. The ratio

187   method assumes constant emissions for VOCs. However, the emission of isoprene greatly

188   depends on temperature and solar irradiation intensity (Zhang et al., 2021b). In addition to

189   accounting for photochemical loss, additional correction of daytime isoprene concentrations

190   was performed using the average diurnal flux of isoprene emissions (Figure S8) (Zhang et al.,

191   2021b). The emission of isoprene showed a clear unimodal curve, and the volume

192   concentration of isoprene was calculated based on the daily emission curve using Eq. (S1).

193   **2.3 Observation-based model simulation**

194   A box model based on the Master Chemical Mechanism (MCM3.3.1) and the Regional

195   Atmospheric Chemical Mechanism (RACM2) was used in this study. The MCM3.3.1 was used

196   to understand the instantaneous ozone formation process, and the RACM2 was used to depict

197   the ozone isopleth due to its high computational efficiency (Sect. 2.4). Table S1 shows the

198   model inputs. The model calculations were constrained with the measured meteorological

199   parameters (RH, T, P, and J_{NO2}) and the concentrations of trace gases, including inorganic

200 species (NO, NO_2, CO, SO_2, and HONO) and 61 organic species (NMHCs (46), OVOCs (8),

201 and halohydrocarbons (7)). The model was validated using the observed and simulated O_3

202 concentrations, which showed good consistency, as shown in Figure S9. The slope and

203 correlation coefficients were 0.9 and 0.8, respectively (Figure S10), respectively, indicating the

204 validity of the model simulation. It is worth mentioning that the results of model simulation

205 can sometimes be overestimated or underestimated to some extent, which has also been

206 reported by previous studies (Zong et al., 2018; Zhang et al., 2020), but this did not affect our

207 simulations of the ozone formation process and mechanisms because we constrained the ozone

208 concentration during our simulations.

209   The ozone formation rate P(O_3) can be quantified by the oxidation rate of NO to NO_2 by

210 peroxyl radicals (Tan et al., 2019), as expressed in Eq. (3). In this study, the modelled peroxyl

211 radical concentrations were used to calculate the ozone production rate.

212     $$P(O_3) = k_{HO_2+NO}[HO_2][NO] + k_{RO_2+NO}[RO_2][NO] \quad (3)$$

213 where $P(O_3)$ is the ozone formation rate; $[HO_2]$ and $[RO_2]$ are the number concentrations of

214 HO_2 and RO_2 radicals; k_{HO2+NO} is the second reaction rate between HO_2 and NO; and k_{RO2+NO}

215 is the second reaction rate for the reaction of RO_2 and NO, which only produces RO and NO_2.

216 Once ozone forms, it will be consumed by OH, HO_2, and alkenes. Additionally, some NO_2 can

217 react with OH, resulting in the formation of nitrate before photolysis. The chemical loss of both

218 O_3 and NO_2 is considered in the calculation of the net ozone production rate (Tan et al., 2019),

219    $$L(O_3) = \left(k_{O_3+OH}[OH] + k_{O_3+HO_2}[HO_2] + k_{O_3+alkenes}[alkenes]\right)[O_3] +$$

220        $$k_{NO_2+OH}[NO_2][OH] \quad (4)$$

221   where $L(O_3)$ is the ozone chemical loss rate; $[OH]$ is the number concentration of OH radical;

222   k_{O3+OH}, k_{O3+HO2}, and $k_{O3+alkenes}$ are the second reaction rates between O_3 and OH, HO_2 and

223   alkenes, respectively; and k_{NO2+OH} is the second reaction rate between NO_2 and OH. Finally,

224    $F(O_3)$ is the net ozone formation rate calculated by the difference between $P(O_3)$ and $L(O_3)$, as

225   expressed in Eq. (5),

$$F(O_3) = P(O_3) - L(O_3) \quad (5)$$

226

2.4 Empirical Kinetic Modelling Approach

227

228   The empirical kinetic modelling approach (EKMA) used in this work is a set of imaginary

229   tests to reveal the dependence of photochemical oxidation products on the change in precursors.

230   We set up 30×30 matrices by reducing or increasing the measured VOCs and NOx

231   concentrations in the model input. The resulting radical concentrations and ozone production

232   rates were calculated correspondingly.

233   At this stage, the observed VOCs were grouped into different lumped species according

234   to their RACM2 classification; more details can be found in a previous publication (Tan et al.,

235   2017). The chemical model simulated photochemical reactions with input species for a time

236   interval of 60 minutes, which was enough for NOx, OH, HO$_2$, and RO$_2$ to reach a steady state

237   because the typical relaxation time of the chemical system is 5-10 minutes in summer (Tan et

238   al., 2018). However, all the species and parameters were input at a 5 min interval by data

239   interpolation to reduce simulation inconsistencies and large distortions of meteorological

240   parameters at longer time intervals (Tan et al., 2018). The ozone production rate was calculated

241   as described in Sect. 2.3. It is worth mentioning that the average survey data were selected as

242 the baseline scenario in simulating the EKMA curve in this study.

3. Results and discussion

3.1 Overview of diurnal variation in O_3, NOx, and TVOC

245   Figure 1 shows the average diurnal variation of concentrations in O_3, NOx, and TVOC

246 (including alkanes, alkenes, OVOCs, and halohydrocarbons) driven by emissions,

247 photochemical reactions and the evolution of the mixing layer height (MLH). The ozone

248 concentration during the observation period was 44.8±27.2 ppb with a maximum of 119.1 ppb,

249 as reported in our previous study (Zhan et al., 2021), which was generally comparable with the

250 O_3 concentrations during 2014-2018 (Ma et al., 2020). The O_3 followed a unimodal curve with

251 a minimum value (18.8±15.4 ppb) at 07:00 and then it increased to a maximum value (69.6

252 ppb) at 15:00 as photochemical ozone formed. In contrast, NOx reached its maximum

253 concentration (39.7±14.2 ppb) at 07:00 and then decreased. After 07:00, the mixing ratio of

254 NO continuously dropped, while the concentration of NO_2 decreased at first and then started

255 to increase at 14:00. The diurnal variations in the observed TVOCs were generally consistent

256 with those of NO_2. The observed TVOCs concentrations ranged from 2.2 to 23.2 ppb, with a

257 mean value of 18.6±2.6 ppb. Compared to the concentrations (45.4±15.2 ppb) in the same

258 period in August 2015 (Li et al., 2016a), the concentration of VOCs in Beijing was effectively

259 reduced. However, the photochemical initial concentrations (PICs) of TVOCs, which varied

260 from 2.2 to 27.8 ppb with a mean value of 24.5±2.1 ppb, showed a different diurnal curve

261 compared with the observed concentrations. It slightly increased from 07:00 to 14:00, which

262 was similar to the diurnal variation of VOCs in previous work (Zhan et al., 2021). The average

PIC-VOCs was 6.9±0.5 ppb higher than the observed concentration of TVOCs, indicating an

underestimated contribution of the local photochemistry of VOCs to O₃ and organic aerosol

formation.
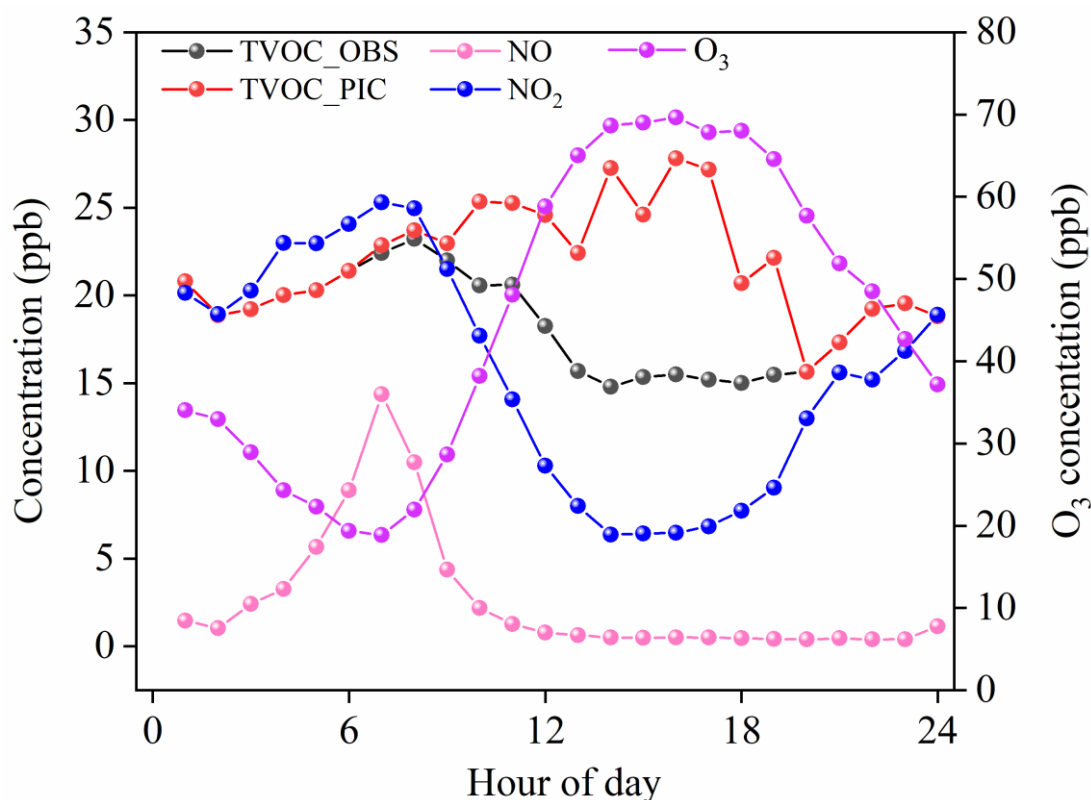
Figure. 1. Overview of average diurnal variations in O₃, NO*x*, and TVOC. The data represent

measured results, except for those of the TVOC_PIC, which are calculated based on OH radical

exposure. The data range is August 1-28, 2019.

3.2 Influence of photochemical loss of VOCs on the O₃ formation sensitivity regime

The sensitivity of O₃ formation is analysed using the isopleth diagram generated from the

EKMA model, which is widely used to qualitatively study O₃-NO*x*-VOCs sensitivity. As

described in Sect. 2.4, the concentrations of NO₂ and VOCs were artificially scaled to ±75%

of the observed values to calculate the response of O₃ concentration to an imaginary change in

the concentrations of NO₂ and VOC, with other constrained conditions remaining unchanged.

276   Figure 2 shows the typical EKMA curves during our observations. The black stars and

277   pentagons denote the observed concentrations of NOx and VOCs in the morning (09:00-10:00)

278   and at noon (14:00-15:00), respectively, while the blue symbols are the corresponding values

279   of PICs. Based on the measured data, O$_3$ formation was in a VOC-limited regime in the

280   morning and a NOx-limited regime in the afternoon. The black arrow indicates a linearly

281   decreasing trend of NOx and VOCs from 09:00 to 15:00 in the chemical coordinate system,

282   and ozone production shifted from VOC-limited to NOx-limited conditions from morning to

283   afternoon, which was consistent with the mean diurnal profiles (Figure 1). This was similar to

284   the data reported in Wangdu (Tan et al., 2018). As expected, ozone production shifted from a

285   VOC-limited regime (the observed VOCs) to a transition regime based on the PIC-VOCs in

286   the morning. Ozone production clearly moved further to a NOx-limited regime in the afternoon

287   after the photochemically consumed NOx and VOCs had been accounted for (Figure 2).

288   Because the average photochemical ageing time was only 1.7±0.9 h, these results indicated

289   that the O$_3$ formation mechanism might typically be misdiagnosed, which misleads mitigation

290   measures for O$_3$ prevention if the consumed VOCs under real atmospheric conditions are not

291   considered.
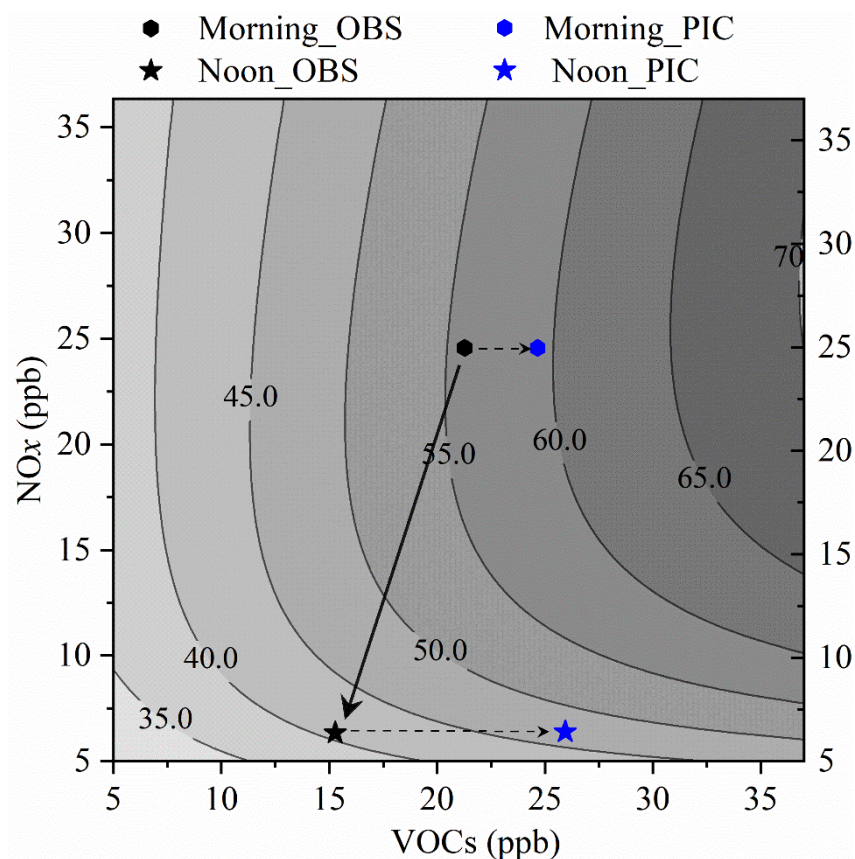
Figure 2. Isopleth diagram of the ozone concentration as a function of the concentration of

NO*x* and VOCs derived from an empirical kinetic modelling approach. The pentagons and stars

indicate the status in the morning (09:00-10:00) and at noon (14:00-15:00), respectively. The

black and blue colours represent the observed and corrected statuses, respectively.

3.3 Contribution of VOC species to O$_3$ production

The time series of simulated OH, HO$_2$, and RO$_2$ concentrations were used to calculate the

$P(O_3)$ and $L(O_3)$. The diurnally averaged $P(O_3)$ and $L(O_3)$ are shown in Figure 3. Ozone

formation can be divided into processes related to RO$_2$+NO and HO$_2$+NO (Sect. 2.3).

According to their VOC precursors, peroxyl radical groups were divided into alkane-derived

(ALKAP), alkene-derived (ALKEP), aromatic-derived (AROMP), isoprene-derived (ISOP),

oxygenated-VOC-derived (OVOCP), and halohydrocarbon-derived (HALOP) RO$_2$ and HO2P.

304   The ozone destruction processes included the reaction between O_3 and HOx (O3D1), the

305   reaction between O1D and H_2O (O3D2), the reaction between O_3 and alkenes (O3D3), and the

306   reaction between NO_2 and OH (O3D4).

307   Based on the observed VOCs (or PIC-VOCs), a fast O_3 production rate was observed at

308   14:00 (or 13:00), with a diurnal maximum value of 16.1 (or 25.6) ppb h^{-1} (Figure 3a and 3b),

309   while the peak destruction rate was 6.4 (or 8.6) ppb h^{-1} at 15:00 (or 13:00) (Figure 3c and 3d).

310   The average daytime $P(O_3)$ from 07:00 to 19:00 based on the initial concentrations of VOCs

311   was 4.0±3.1 ppb h^{-1} higher than that based on the measured VOCs concentrations (Figure 3b).

312   At the same time, the $F(O_3)$ from 07:00 to 19:00 based on the initial concentrations of VOCs

313   was also 3.0±2.1 ppb h^{-1} higher than the measured counterpart (Figure S11). Thus, the net O_3

314   production could be accumulatively underestimated by ~36 ppb day^{-1} from 07:00 to 19:00 if

315   the consumption of VOCs was not considered. This meant that the contribution of the local

316   formation of O_3 could be underestimated using the directly measured VOCs concentrations. It

317   should be pointed out that it is better to compare O_3 production with the true metric for O_3

318   production. However, it is impossible to directly measure the true metric for O_3 production in

319   the atmosphere at the present time to know how well the method presented here corrects for

320   that underestimation. In addition, the ozone concentrations must be constrained when

321   simulating the ozone formation process (Lu et al., 2013; Tan et al., 2017). Thus, it is impossible

322   to directly compare the ozone production based on PIC-VOCs with that using measured VOCs

323   concentrations. Therefore, we alternatively compared the integrated net ozone production rates

324   rather than ozone production or concentrations between the two scenarios. An upwind O_3 and

325 VOCs measurement combined with a trajectory analysis might provide an approach for

326 checking the accuracy of our results. Alternatively, conducting a transient O_3 production rate

327 analysis after subtracting the transport of O_3 with a regional model and/or satellite observation

328 might be another option. Unfortunately, neither the upwind measurement nor the regional

329 model simulation was available at the time of our study. To further check the accuracy of our

330 results, we chose August 4th as a test case to explore the influence of the transport of ozone on

331 a downwind site based on the trajectory analysis. As shown in Figure S12, the mean ozone

332 concentration of the downwind site (national monitoring station, NMS) was 27.6±21.9 ppb

333 day^{-1} higher than that of the observation site (OS), which was slightly less than the difference

334 (~36 ppb day^{-1}) between PIC-VOCs and observed VOCs and indirectly rationalized our results.

335   The HO_2 path contributed 64.8% to the total ozone formation on average, which was

336 slightly higher than the reported value (57.0%) in Wangdu (Tan et al., 2018), whereas the RO_2

337 path, in which aromatics (9.4%), alkenes (8.4%), isoprene (7.8%), alkanes (4.7%), OVOCs

338 (4.3%) and halohydrocarbons (0.6%) were the main contributors, contributed to the remaining

339 part. For the PIC-VOCs, the dominant path of O_3 production (51.7%) was still the HO_2 path,

340 followed by the RO_2 path related to alkenes (14.7%), aromatics (12.8%), and isoprene (11.7%).

341 The relative contribution of the RO_2 path to $P(O_3)$ increased by 13.4% compared with the

342 measured VOCs, particularly alkene-derived RO_2, which increased by 10.2%. As shown in

343 Figure 3c and 3d, the destruction of total oxidants was dominated by the reaction between O_3

344 and alkenes (O3D3) in the morning. It gradually shifted to the reaction between NO_2 and OH

345 (O3D4) from 11:00 to 16:00 and the photolysis of O_3 followed by a reaction with water (O3D2)

346 from 12:00 to 15:00 because O₃ concentration increased while NO₂ decreased (Figure 3c).

347 Figure S13 shows the percentages of the different paths of P(O₃) and L(O₃). The relative

348 contributions of the reactions between O₃ and alkenes (O1D3) and between NO₂ and OH

349 (O1D4) to the O₃ sinks decreased when calculated based on PIC-VOCs compared with those

350 of the measured VOCs, while they obviously increased for the other two paths, i.e., O3D1 and

351 O3O2. The O₃ destruction of the HOx and O₃ reaction (O3D1) gradually increased with the

352 continuous photochemical reaction. In addition, the maximum O₃ formation rates of the RO₂

353 derived from OVOCs and halohydrocarbons were 0.75 and 0.18 ppb h⁻¹, respectively. These

354 values could be underestimated due to the incomplete gas reaction mechanism of OVOCs and

355 halohydrocarbons in MCM3.3.1. In general, the measured VOCs as model inputs could fail to

356 truly reflect the oxidation capacity and underestimate the local formation of O₃ and organic

357 aerosols (Zhan et al., 2021).
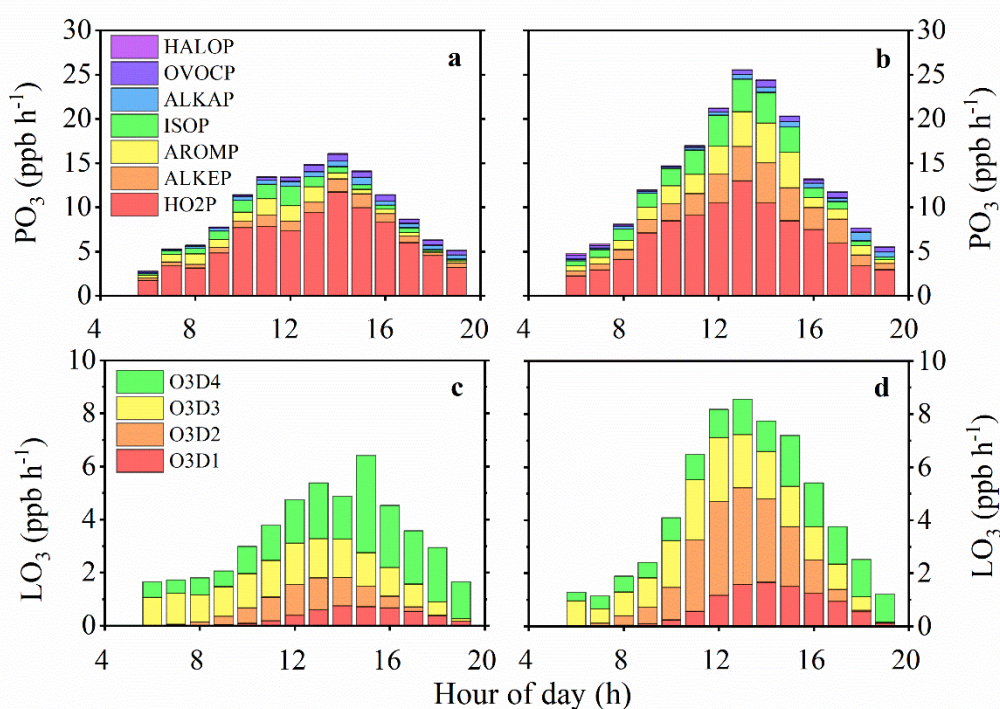
358

359   **Figure 3.** Mean diurnal profile of the instantaneous ozone production and destruction rate

360   calculated from the MCM-OBM model (instantaneous ozone rate derived from observed VOCs

361   in a and c and from PIC-VOCs in b and d). The upper panel presents the speciation of the ozone

362   formation rate. The lower panel presents the speciation of the ozone destruction rate. The data

363   range is August 1-28, 2019.

364

365   The budget of OH-HO_2-RO_2 radicals was further analysed to understand the

366   photochemical O_3 formation process. The comparison of the radical budget derived from the

367   observed and PIC-VOCs is shown in Figure 4. The radical cycles are divided into radical

368   sources (green boxes), radical sinks (black boxes), radical propagations (red circles) and

369   equilibria between radical and reservoir species (yellow boxes). The numbers or percentages

370   are the average formation rates (ppb h^{-1}) or relative contributions of the corresponding reaction

371   path based on the observed VOCs (outside the brackets) and the PIC-VOCs (inside the brackets)

372   to a certain radical. The relative contributions of different radical paths based on the observed

373   VOCs (outside the brackets) were comparable with those reported in Beijing, Shanghai, and

374   Guangzhou (Tan et al., 2019), while variations were observed for some reaction paths based

375   on the PIC-VOCs. For example, the reaction between ozone and alkenes based on initial VOC

376   concentrations (percentages inside the brackets) contributed more to OH (from 7% to 21%)

377   and HO_2 radical production (from 6% to 12%), while photolysis of HONO and HCHO

378   contributed less to the production of OH (from 76% to 60%) and HO_2 radicals (from 44% to

379   40%), respectively. Other radical sources were consistent between the two scenarios.

380   Interestingly, the average formation rates of OH, HO_2 and RO_2 radicals derived from the PIC-

381   VOCs were obviously higher than those from the observed VOCs. In particular, the oxidation

382   of NO by RO_2 and HO_2 increased by 1.6 and 1.3 ppb h^{-1}, respectively. The enhanced oxidation

383   rate of NO was equal to the increase in the average $F(O_3)$ in the analysis process above. This

384   meant that the radical propagation of OH-RO_2-HO_2 sped up in the case of PIC-VOCs,

385   subsequently accelerating the chemical loop of NO-NO_2-O_3. For the radical sinks and equilibria

386   related to HNO_4, $RONO_2$ and PAN, the values were basically comparable between the two

387   scenarios. In addition, the O_3 formation from the RO_2 path increased by 4.1% (from 39.5% to

388   43.6%) in the simulation using the PIC-VOCs compared with the observed VOCs. The above

389   budget analysis explained the observed increases in $F(O_3)$ (~3 ppb h^{-1}), which were mainly

390   driven by the reaction of missed reactive VOCs, such as alkenes, with O_3.
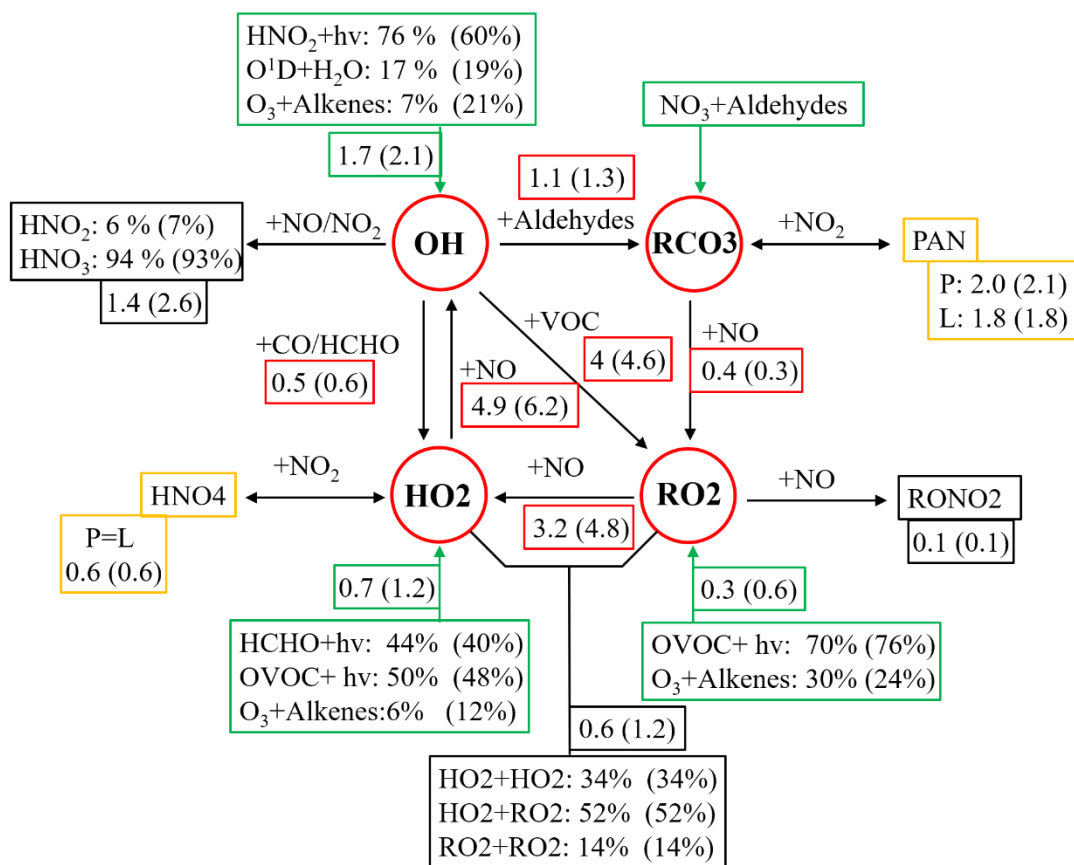
391

392   **Figure 4.** Comparison of the OH-HO_2-RO_2 radical budget derived from the observed and PIC-

393   VOCs under daytime conditions (07:00 to 19:00 LT). The green, black, red and yellow boxes

394   denote the sources of radicals, radical sinks, radical propagation, and racial equilibrium,

395   respectively. The numbers or percentages outside and inside the brackets are the average

396   formation rates (ppb h^{-1}) or relative contributions to a specific radical of the corresponding

397   reaction path based on observed VOCs and PIC-VOCs, respectively.

398   **3.4 In situ O$_3$ formation process**

399   In addition to chemical processes, which can be simulated using the OBM-MCM model,

400   transport processes, including horizontal, vertical transportation and dry deposition processes

401   (Tan et al., 2019), also have an important influence on the O$_3$ concentration. Thus, the change

402   in instantaneous ozone concentration can reflect the combined effect between photochemical

403   and physical transport processes (Tan et al., 2019). This change can be expressed as,

404
$$\frac{dO_x}{dt} = F(O_3) + R(O_3) \quad (6)$$

405   where dOx/dt is the O$_3$ concentration change rate based on the measured data (ppb h^{-1}); $F(O_3)$

406   is the net O$_3$ formation rate (ppb h^{-1}), and $R(O_3)$ indicates transportation (ppb h^{-1}). A positive

407   value of $R(O_3)$ indicates an inflow of O$_3$ with airmass and vice versa. O$_3$ was replaced with Ox

408   (O$_3$+NO$_2$) to correct the titration of O$_3$ by NO (Pan et al., 2015).

409
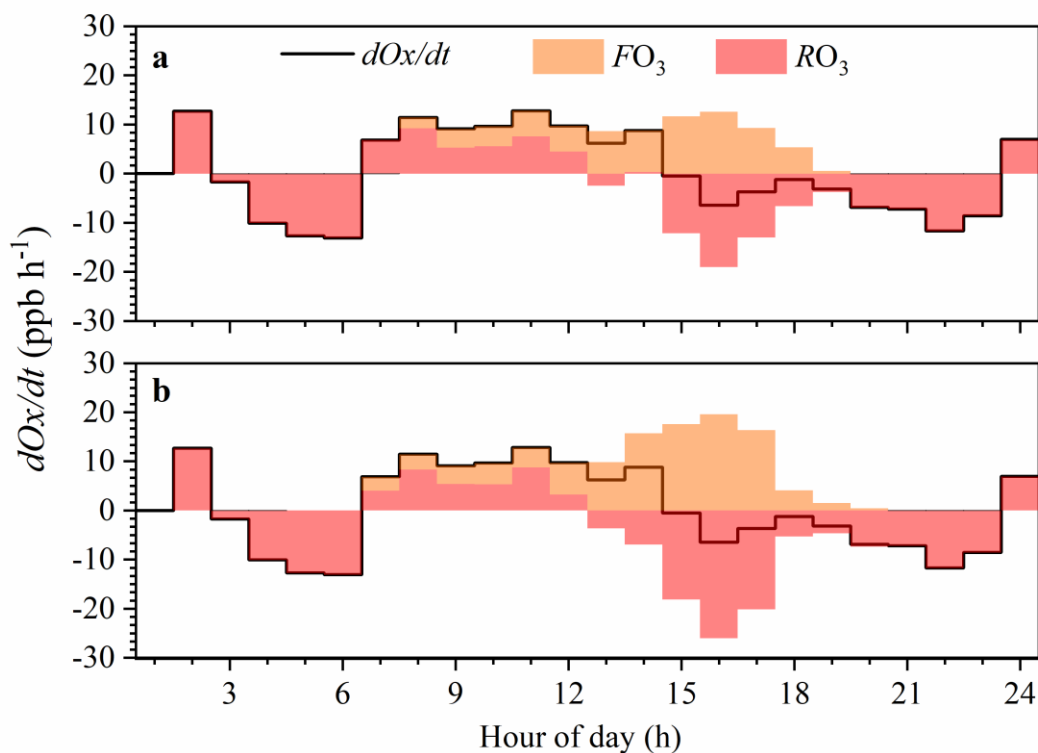
Fig. 5. The variation in Ox concentration and formation rate during an O_3 pollution episode

(Aug. 1st). (a and b present the local ozone formation processes of the measured and PIC-VOCs,

respectively.)

The O_3 budget analysis was performed during an O_3 pollution episode (Aug. 1st). Figure

5 shows the simulated local ozone formation process based on the measured and PIC-VOCs.

The hourly variation in O_3 concentrations from 19:00 to 6:00 the next day was dominated by

regional transportation without O_3 formation, while local photochemical O_3 formation could

explain all or part of the O_3 concentration change during the time window from 07:00 to 19:00.

The $d(O_3)/dt$ shows an increase from 07:00 to 15:00 LT. However, $d(O_3)/dt$ sharply changed to

negative values at 16:00, which was consistent with diurnal O_3 (the O_3 peaks at 15:00) in Figure

1.

421   The average daytime $F(O_3)$ based on the observed and photochemical initial

422   concentrations was 6.4±4.0 and 8.9±6.7 ppb h^{-1}, respectively. Photochemical O_3 formation

423   under both conditions started at 07:00 and reached maximum values of 12.6 and 19.6 ppb h^{-1}

424   at 15:00, respectively. The maximum daily value of $P(O_3)$ was higher than those in the urban

425   areas of Japan, America, and England (Whalley et al., 2018; Ren et al., 2006; Griffith et al.,

426   2016; Kanaya et al., 2009) and lower than those in the suburbs of Guangzhou (Lu et al., 2012)

427   and the urban areas and suburbs of Beijing (Lu et al., 2013). Before 12:00, the O_3 formation

428   rate based on the PIC-VOCs was slightly higher than that based on the measured VOCs, while

429   both rates were within a range of 2.0~6.5 ppb h^{-1}. From 12:00 to 17:00, the O_3 formation rate

430   based on the PIC-VOCs and the observed concentration of VOCs greatly increased due to

431   active photochemistry.

432   As shown in Figure 5, the increased O_3 concentration was larger than the local O_3

433   photochemical production from 07:00 to 12:00 ($R(O_3)$ was positive). This was mainly because

434   the residual layer (RL) that formed at night was unfavourable for the inversion of airmass in

435   the early morning (Tan et al., 2021). The RL usually contains an airmass with a higher

436   concentration of O_3 than that in the nocturnal boundary layer. Vertical transport becomes

437   prominent due to the fast entrainment when the boundary layer is gradually uplifted. However,

438    $R(O_3)$ was negative in the afternoon, which indicated that the local O_3 formation at the

439   measurement site contributed to not only the changes in the in situ O_3 concentration but also

440   the O_3 source of the downwind regions. This was more clearly shown in Figure 4B under the

441   PIC-VOCs condition. These results illustrated that local O_3 photochemistry played a crucial

442 role in both the local and regional O_3 concentrations, which can be underestimated if consumed

443 VOCs with high reactivities are ignored.

4. Conclusions

445 In this study, we presented the local O_3 formation process in August 2019 in Beijing based

446 on the concentrations of observed and PIC-VOCs. The mean diurnal profile of O_3 was

447 unimodal with a peak at 15:00, while NOx and observed TVOCs showed an opposite diurnal

448 curve, and the PICs of TVOCs showed a different diurnal curve compared with that of the

449 observed VOCs, with a slight increase from 07:00 to 14:00. The EKMA curve indicated that

450 instantaneous O_3 production was dependent on the real-time concentrations of NOx and VOCs,

451 i.e., the VOC-limited regime in the morning (09:00-10:00) and the NOx-limited regime at noon

452 (14:00-15:00). The sensitivity regime of O_3 formation could be misdiagnosed if the consumed

453 VOCs are not considered, for example, the VOC-limited regime (observed) shift to a transition

454 regime (PIC-VOCs) in the morning is ignored. The mean $F(O_3)$ based on PIC-VOCs was 3.0

455 ppb h^{-1} higher than that based on the measured VOCs, indicating that the underestimation of

456 local photochemistry in the local O_3 concentration could reach ~36 ppb day^{-1} if the consumed

457 VOCs are not accounted for. The radical budget analysis explained the observed increases in

458 $F(O_3)$ (3 ppb h^{-1}), which were mainly driven by the reaction of missed reactive VOCs, such as

459 alkenes, with O_3. In addition, the OH-HO$_2$ radical cycle was obviously accelerated by highly

460 reactive alkenes after the photochemical loss of VOCs was accounted for. Finally, the results

461 of the in situ O_3 formation process indicated that local O_3 photochemical formation played a

462 key role in both local and regional O_3 concentrations. In conclusion, our results suggested that

463   PIC-VOCs were more suitable than the observed VOC concentrations for diagnosing O_3

464   formation sensitivity.

465

466   **Author contributions:** Wei Ma: Methodology, data curation, and writing of the original draft;

467   Zemin Feng: Methodology, investigation, data curation, and writing of the original draft; Junlei

468   Zhan: Methodology, investigation, data curation; Yongchun Liu: Conceptualization,

469   investigation, data curation, writing, reviewing & editing, supervision, and funding acquisition;

470   Pengfei Liu: Methodology, investigation, data curation, writing, reviewing & editing;

471   Chengtang Liu: Methodology, investigation, data curation, writing, reviewing & editing;

472   Qingxin Ma: Methodology, investigation, data curation; Kang Yang: Methodology,

473   investigation, data curation. Yafei Wang: Methodology, investigation, resources, data curation;

474   Hong He: Resources, writing, reviewing & editing; Markku Kulmala: Methodology, writing,

475   reviewing & editing; Yujing Mu: Conceptualization, methodology, data curation, writing,

476   reviewing & editing. Junfeng Liu: Conceptualization, methodology, data curation, writing,

477   reviewing & editing, and supervision.

478   **Competing interests:** The authors declare that they have no substantive conflicts of interest.

479   **Data availability:** Data are available upon request to Yongchun Liu (liuyc@buct.edu.cn).

480   **Acknowledgements:** This research was financially supported by the National Natural Science

481   Foundation of China (41877306, 92044301, 21976190), the Ministry of Science and

482   Technology of the People's Republic of China (2019YFC0214701), the Strategic Priority

483   Research Program of the Chinese Academy of Sciences and Beijing University of Chemical

484   Technology.

485

486

Reference

Atkinson, R. and Arey, J.: Atmospheric degradation of volatile organic compounds, Chemical Reviews, 103, 4605-4638, https://doi.org/10.1021/cr0206420, 2003.

Carter, W. P. L.: Development of Ozone Reactivity Scales for Volatile Organic Compounds.   1994a, J. Air Waste Manage. Assoc., 44, 881-899, https://doi.org/10.1080/1073161X.1994.10467290, 1994.

Chen, T., Liu, J., Liu, Y., and Ma, Q. G., Yanli; Zhong,Cheng; Jiang,Haotian; Chu,Biwu; Zhang,Peng; Ma,Jinzhu; Liu,Pengfei; Wang,Yafei; Mu,Yujing; He,Hong: Chemical characterization of submicron aerosol in summertime Beijing: A case study in southern suburbs in 2018, Chemosphere, 247, 125918, https://doi.org/10.1016/j.chemosphere.2020.125918, 2020.

Cohen, A. J., Brauer, M., Burnett, R., and Anderson, H. R. F., Joseph; Estep,Kara; Balakrishnan,Kalpana; Brunekreef,Bert; Dandona,Lalit; Dandona,Rakhi; Feigin,Valery; Freedman,Greg; Hubbell,Bryan; Jobling,Amelia; Kan,Haidong; Knibbs,Luke; Liu,Yang; Martin,Randall; Morawska,Lidia; Pope,C. Arden, III; Shin,Hwashin; Straif,Kurt; Shaddick, Gavin; Thomas,Matthew; van Dingenen,Rita; van Donkelaar,Aaron; Vos,Theo; Murray,Christopher J. L; Forouzanfar,Mohammad H.: Estimates and 25-year trends of the global burden of disease attributable to ambient air pollution: an analysis of data from the Global Burden of Diseases Study 2015, Lancet, 389, 1907-1918, https://doi.org/10.1016/s0140-6736(17)30505-6, 2017.

Dang, R. and Liao, h.: Radiative Forcing and Health Impact of Aerosols and Ozone in China as the Consequence of Clean Air Actions over 2012–2017, J Geophysical Research Letters, 46, 12511-12519, https://doi.org/10.1029/2019GL084605, 2019.

Feng, Z., De Marco, A., Anav, A., Gualtieri, M., Sicard, P., Tian, H., Fornasier, F., Tao, F., Guo, A., and Paoletti, E.: Economic losses due to ozone impacts on human health, forest productivity and crop yield across China, Environment International, 131, 104966, https://doi.org/10.1016/j.envint.2019.104966, 2019.

Gao, J., Zhang, J., Li, H., Li, L., and Xu, L. Z., Yujie; Wang,Zhanshan; Wang,Xuezhong; Zhang,Weiqi; Chen,Yizhen; Cheng,Xi; Zhang,Hao; Peng,Liang; Chai,Fahe; Wei,Yongjie: Comparative study of volatile organic compounds in ambient air using observed mixing ratios and initial mixing ratios taking chemical loss into account - A case study in a typical urban area in Beijing, Science of the Total Environment, 628-629, 791-804, https://doi.org/10.1016/j.scitotenv.2018.01.175, 2018.

Gao, Y., Li, M., Wan, X., Zhao, X., Wu, Y., Liu, X., and Li, X.: Important contributions of alkenes and aromatics to VOCs emissions, chemistry and secondary pollutants formation at an industrial site of central eastern China, Atmospheric Environment, 244, 117927, https://doi.org/10.1016/j.atmosenv.2020.117927, 2021.

Goldan, P. D., Parrish, D. D., Kuster, W. C., Trainer, M., Mckeen, S. A., Holloway, J., Jobson, B. T., Sueper, D. T., and Fehsenfeld, F. C.: Airborne measurements of isoprene, CO, and anthropogenic hydrocarbons and their implications, Journal of Geophysical Research-Atmospheres, 105, 9091-9105, http://doi.org/10.1029/1999JD900429, 2000.

Griffith, S. M., Hansen, R. F., Dusanter, S., Michoud, V., Gilman, J. B., Kuster, W. C., Veres, P. R., Graus, M., de Gouw, J. A., Roberts, J., Young, C., Washenfelder, R., Brown, S. S., Thalman, R., Waxman, E., Volkamer, R., Tsai, C., Stutz, J., Flynn, J. H., Grossberg, N., Lefer, B., Alvarez, S. L., Rappenglueck, B., Mielke, L. H., Osthoff, H. D., and Stevens, P. S.: Measurements of hydroxyl and hydroperoxy radicals during CalNex-LA: Model comparisons and radical budgets, Journal of Geophysical Research-Atmospheres, 121, 4211-4232, https://doi.org/10.1002/2015jd024358, 2016.

Han, D., Wang, Z., Cheng, J., Wang, Q., Chen, X., and Wang, H.: Volatile organic compounds (VOCs) during

non-haze and haze days in Shanghai: characterization and secondary organic aerosol (SOA) formation, Environmental Science and Pollution Research, 24, 18619-18629, https://doi.org/10.1007/s11356-017-9433-3, 2017.

He, Z., Wang, X., Ling, Z., Zhao, J., Guo, H., Shao, M., and Wang, Z.: Contributions of different anthropogenic volatile organic compound sources to ozone formation at a receptor site in the Pearl River Delta region and its policy implications, Atmospheric Chemistry and Physics, 19, 8801-8816, https://doi.org/10.5194/acp-19-8801-2019, 2019.

Jobson, B. T., Berkowitz, C. M., Kuster, W. C., Goldan, P. D., Williams, E. J., Fesenfeld, F. C., Apel, E. C., Karl, T., Lonneman, W. A., and Riemer, D.: Hydrocarbon source signatures in Houston, Texas: Influence of the petrochemical industry, Journal of Geophysical Research-Atmospheres, 109, http://doi.org/10.1029/2004jd004887, 2004.

Kanaya, Y., Pochanart, P., Liu, Y. L., J;, Tanimoto, H., Kato, S., Suthawaree, J., Inomata, S., Taketani, F., Okuzawa, K., Kawamura, K., Akimoto, H., and Wang, Z. F.: Rates and regimes of photochemical ozone production over Central East China in June 2006: a box model analysis using comprehensive measurements of ozone precursors, Atmospheric Chemistry and Physics, 9, 7711-7723, https://doi.org/10.5194/acp-9-7711-2009, 2009.

Li, J., Wu, R., Li, Y., Hao, Y., and Xie, S. Z., Liming;: Effects of rigorous emission controls on reducing ambient volatile organic compounds in Beijing, China, Science of the Total Environment, 557, 531-541, https://doi.org/10.1016/j.scitotenv.2016.03.140, 2016a.

Li, J., Yang, W., Wang, Z., Chen, H., Hu, B., Li, J., Sun, Y., Fu, P., and Zhang, Y.: Modeling study of surface ozone source-receptor relationships in East Asia, Atmospheric Research, 167, 77-88, https://doi.org/10.1016/j.atmosres.2015.07.010, 2016b.

Li, L., An, J. Y., Shi, Y. Y., and Zhou, M. Y., R. S; Huang, C; Wang, H. L; Lou, S. R; Wang, Q; Lu, Q; Wu, J.: Source apportionment of surface ozone in the Yangtze River Delta, China in the summer of 2013, Atmospheric Environment, 144, 194-207, https://doi.org/10.1016/j.atmosenv.2016.08.076, 2016c.

Li, M., Zhang, Q., Zheng, B., Tong, D., Lei, Y., Liu, F., Hong, C., Kang, S., Yan, L., Zhang, Y., Bo, Y. S., Hang;, Cheng, Y., and He, K.: Persistent growth of anthropogenic non-methane volatile organic compound (NMVOC) emissions in China during 1990-2017: drivers, speciation and ozone formation potential, Atmospheric Chemistry and Physics, 19, 8897-8913, https://doi.org/10.5194/acp-19-8897-2019, 2019.

Ling, Z. H. and Guo, H.: Contribution of VOC sources to photochemical ozone formation and its control policy implication in Hong Kong, Environmental Science & Policy, 38, 180-191, https://doi.org/10.1016/j.envsci.2013.12.004, 2014.

Liu, J., Li, X., Tan, Z., Wang, W., and Zhang, Y.: Assessing the Ratios of Formaldehyde and Glyoxal to NO_2 as Indicators of O_3–NO_x–VOC Sensitivity, Environmental Science Technology, 55, 10935-10945, https://doi.org/10.1021/acs.est.0c07506, 2021.

Liu, Y., Yan, C., Feng, Z., Zheng, F., and Kulmala, M.: Continuous and comprehensive atmospheric observations in Beijing: a station to understand the complex urban atmospheric environment, Big Earth Data, 4, 295-321, https://doi.org/10.1080/20964471.2020.1798707, 2020a.

Liu, Y., Ni, S., Jiang, T., Xing, S., Zhang, Y., Bao, X., Feng, Z., Fan, X., Zhang, L., and Feng, H.: Influence of Chinese New Year overlapping COVID-19 lockdown on HONO sources in Shijiazhuang, Science of the Total Environment, 745, 141025, https://doi.org/10.1016/j.scitotenv.2020.141025, 2020b.

Liu, Y., Zhang, Y., Lian, C., Yan, C., Feng, Z., Zheng, F., Fan, X., Chen, Y., Wang, W., Chu, B., Wang, Y., Cai, J., Du, W., Daellenbach, K. R., Kangasluoma, J., Bianchi, F., Kujansuu, J., Petaja, T., Wang, X., Hu, B., Wang, Y.,

Ge, M., He, H., and Kulmala, M.: The promotion effect of nitrous acid on aerosol formation in wintertime in Beijing: the possible contribution of traffic-related emissions, Atmospheric Chemistry and Physics, 20, 13023-13040, https://doi.org/10.5194/acp-20-13023-2020, 2020c.

Lu, K. D., F. Rohrer; F. Holland, H. F., B. Bohn,T. Brauers,C. C. Chang,R. Haseler ,M. Hu,K. Kita, and , Y. K., X. Li,S. R. Lou,S. Nehr,M. Shao,L. M. Zeng,A. Wahner,Y. H. Zhang,and A. Hofzumahaus: Observation and modelling of OH and HO2 concentrations in the Pearl River Delta 2006: a missing OH source in a VOC rich atmosphere, Atmospheric Chemistry and Physics, 12, 1541-1569, https://doi.org/10.5194/acp-12-1541-2012, 2012.

Lu, K. D., Hofzumahaus, A., Holland, F., Bohn, B., Brauers, T., Fuchs, H., Hu, M., Haeseler, R., Kita, K., Kondo, Y., Li, X., Lou, S. R., Oebel, A., Shao, M., Zeng, L. M., Wahner, A., Zhu, T., Zhang, Y. H., and Rohrer, F.: Missing OH source in a suburban environment near Beijing: observed and modelled OH and HO_2 concentrations in summer 2006, Atmospheric Chemistry and Physics, 13, 1057-1080, https://doi.org/10.5194/acp-13-1057-2013, 2013.

Lu, X., Chen, N., Wang, Y., Cao, W., Zhu, B., Yao, T., Fung, J. C. H., and Lau, A. K. H.: Radical budget and ozone chemistry during autumn in the atmosphere of an urban site in central China, Journal of Geophysical Research-Atmospheres, 122, 3672-3685, https://doi.org/10.1002/2016jd025676, 2017.

Ma, j. K., Jyoti;, Li, V. O. K., and Lam, J. C. K.: Effects of China's current Air Pollution Prevention and Control Action Plan on air pollution patterns, health risks and mortalities in Beijing 2014-2018, Chemosphere, 260, 127572, https://doi.org/10.1016/j.chemosphere.2020.127572, 2020.

Ma, Z., Liu, C., Zhang, C., Liu, P., Ye, C., Xue, C., Zhao, D., Sun, J., Du, Y., Chai, F., and Mu, Y.: The levels, sources and reactivity of volatile organic compounds in a typical urban area of Northeast China, Journal of Environmental Sciences, 79, 121-134, https://doi.org/10.1016/j.jes.2018.11.015, 2019.

Mckeen, S. A., Liu, S. C., Hsie, E. Y., Lin, X., Bradshaw, J. D., Smyth, S., Gregory, G. L., and Blake, D. R.: Hydrocarbon ratios during PEM-WEST A: A model perspective, Journal of Geophysical Research: Atmospheres, 101, 2087-2109, https://doi.org/10.1029/95JD02733, 1996.

Monks, P. S.: Gas-Phase Radical Chemistry in the Troposphere, Chemical Society Reviews, 34, 376-395, https://doi.org/10.1039/B307982C, 2005.

Pan, X., Kanaya, Y., Tanimoto, H., Inomata, S., Wang, Z., Kudo, S., and Uno, I.: Examining the major contributors of ozone pollution in a rural area of the Yangtze River Delta region during harvest season, Atmospheric Chemistry and Physics, 15, 6101-6111, https://doi.org/10.5194/acp-15-6101-2015, 2015.

Ren, X., Brune, W. H., Mao, J., Mitchell, M. J., Lesher, R. L., Simpas, J. B., Metcalf, A. R., Schwab, J. J., Cai, C., Li, Y., Demerjian, K. L., Felton, H. D., Boynton, G., Adams, A., Perry, J., He, Y., Zhou, X., and Hou, J.: Behavior of OH and HO2 in the winter atmosphere in New York city, Atmospheric Environment, 40, S252-S263, https://doi.org/10.1016/j.atmosenv.2005.11.073, 2006.

Seinfeld, J. H. and Pandis, S. N.: Atmospheric chemistry and physics : from air pollution to climate change (Second Edition), 2006.

Shao, M., Wang, B., Lu, S., Yuan, B., and Wang, M.: Effects of Beijing Olympics Control Measures on Reducing Reactive Hydrocarbon Species, Environmental Science & Technology, 45, 514-519, https://doi.org/10.1021/es102357t, 2011.

Tan, Z., Fuchs, H., Lu, K., and Hofzumahaus, A. B., Birger; Broch,Sebastian; Dong,Huabin; Gomm,Sebastian; Haeseler,Rolf; He,Lingyan; Holland,Frank; Li,Xin; Liu,Ying; Lu,Sihua; Rohrer,Franz; Shao,Min; Wang,Baolin; Wang,Ming; Wu,Yusheng; Zeng,Limin; Zhang,Yinsong; Wahner,Andreas; Zhang,Yuanhang;: Radical chemistry

at a rural site (Wangdu) in the North China Plain: observation and model calculations of OH,HO$_2$ and RO$_2$ radicals, Atmospheric Chemistry and Physics, 17, 663-690, https://doi.org/10.5194/acp-17-663-2017, 2017.

Tan, Z., Lu, K., Jiang, M., Rong, S., and Zhang, Y.: Daytime atmospheric oxidation capacity in four Chinese megacities during the photochemically polluted season: A case study based on box model simulation, Atmospheric Chemistry Physics, 19, 3493-3513, https://doi.org/10.5194/acp-19-3493-2019, 2019.

Tan, Z., Lu, K., Jiang, M., Su, R., Dong, H., Zeng, L., Xie, S., Tan, Q., and Zhang, Y.: Exploring ozone pollution in Chengdu, southwestern China: A case study from radical chemistry to O$_3$-VOC-NOx sensitivity, Science of the Total Environment, 636, 775-786, https://doi.org/10.1016/j.scitotenv.2018.04.286, 2018.

Tan, Z. F., Ma, X. F., Lu, K. D., Jiang, M. Q., Zou, Q., Wang, H. C., Zeng, L. M., and Zhang, Y. H.: Direct evidence of local photochemical production driven ozone episode in Beijing: A case study, Science of the Total Environment, 800, http://doi.org/10.1016/j.scitotenv.2021.148868, 2021.

Wang, T., Xue, L., Brimblecombe, P., Lam, Y. F., Li, L., and Zhang, L.: Ozone pollution in China: A review of concentrations, meteorological influences, chemical precursors, and effects, Science of the Total Environment, 575, 1582-1596, https://doi.org/10.1016/j.scitotenv.2016.10.081, 2017.

Whalley, L. K., Stone, D., Dunmore, R., Hamilton, J., Hopkins, J. R., Lee, J. D., Lewis, A. C., Williams, P., Kleffmann, J., Laufs, S., Woodward-Massey, R., and Heard, D. E.: Understanding in situ ozone production in the summertime through radical observations and modelling studies during the Clean air for London project (ClearfLo), Atmospheric Chemistry and Physics, 18, 2547-2571, https://doi.org/10.5194/acp-18-2547-2018, 2018.

Wiedinmyer, C., Friedfeld, S., Baugh, W., Greenberg, J., Guenther, A., Fraser, M., and Allen, D.: Measurement and analysis of atmospheric concentrations of isoprene and its reaction products in central Texas, Atmospheric Environment, 35, 1001-1013, https://doi.org/10.1016/S1352-2310(00)00406-4, 2001.

Xie, Y., Dai, H., Zhang, Y., Wu, Y., Hanaoka, T., and Masui, T.: Comparison of health and economic impacts of PM2.5 and ozone pollution in China, Environment International, 130, 104881, https://doi.org/10.1016/j.envint.2019.05.075, 2019.

Xue, L. K., Wang, T., Gao, J., Ding, A. J., Zhou, X. H., Blake, D. R., Wang, X. F., Saunders, S. M., Fan, S. J., Zuo, H. C., Zhang, Q. Z., and Wang, W. X.: Ground-level ozone in four Chinese cities: precursors, regional transport and heterogeneous processes, Atmospheric Chemistry and Physics, 14, 13175-13188, https://doi.org/10.5194/acp-14-13175-2014, 2014.

Yang, Y., Shao, M., Kessel, S., Li, Y. L., Keding;, Lu, S. W., Jonathan;, Zhang, Y., Zeng, L., Noelscher, A. C., Wu, Y., Wang, X., and Zheng, J.: How the OH reactivity affects the ozone production efficiency: case studies in Beijing and Heshan, China, Atmospheric Chemistry and Physics, 17, 7127-7142, https://doi.org/10.5194/acp-17-7127-2017, 2017.

Yuan, B., Hu, W. W., Shao, M., Wang, M., Chen, W. T., Lu, S. H., Zeng, L. M., and Hu, M.: VOC emissions, evolutions and contributions to SOA formation at a receptor site in eastern China, Atmospheric Chemistry and Physics, 13, 8815-8832, https://doi.org/10.5194/acp-13-8815-2013, 2013.

Zhan, J., Feng, Z., Liu, P., He, X., He, Z., Chen, T., Wang, Y., He, H., Mu, Y., and Liu, Y.: Ozone and SOA formation potential based on photochemical loss of VOCs during the Beijing summer, Environmental Pollution, 285, 117444, https://doi.org/10.1016/j.envpol.2021.117444, 2021.

Zhang, K., Li, L., Huang, L., Wang, Y., Huo, J., Duan, Y., Wang, Y., and Fu, Q.: The impact of volatile organic compounds on ozone formation in the suburban area of Shanghai, Atmospheric Environment, 232, 117511, https://doi.org/10.1016/j.atmosenv.2020.117511, 2020.

Zhang, K., Huang, L., Li, Q., Huo, J., Duan, Y., Wang, Y., Yaluk, E., Wang, Y., Fu, Q., and Li, L.: Explicit modeling

654 of isoprene chemical processing in polluted air masses in suburban areas of the Yangtze River Delta region: radical

655 cycling and formation of ozone and formaldehyde, Atmospheric Chemistry and Physics, 21, 5905-5917,

656 https://doi.org/10.5194/acp-21-5905-2021, 2021a.

657 Zhang, M., Gao, W., Yan, J., Wu, Y., Marandino, C. A., Park, K., Chen, L., Lin, Q., Tan, G., and Pan, M.: An

658 integrated sampler for shipboard underway measurement of dimethyl sulfide in surface seawater and air,

659 Atmospheric Environment, 209, 86-91, https://doi.org/10.1016/j.atmosenv.2019.04.022, 2019.

660 Zhang, Q., Li, L., Zhao, W., Wang, X., Jiang, L., Liu, B., Li, X., and Lu, H.: Emission characteristics of VOCs

661 from forests and its impact on regional air quality in Beijing, China Environmental Science, 41, 622-632,

662 https://doi.org/10.19674/j.cnki.issn1000-6923.2021.0072, 2021b.

663 Zong, R. H., Xue, L. K., Wang, T. B., and Wang, W. X.: Inter-comparison of the Regional Atmospheric Chemistry

664 Mechanism (RACM2) and Master Chemical Mechanism (MCM) on the simulation of acetaldehyde, Atmospheric

665 Environment, 186, 144-149, http://doi.org/10.1016/j.atmosenv.2018.05.013, 2018.

666